Atmos. Chem. Phys. Discuss., https://doi.org/10.5194/acp-2018-898
Manuscript under review for journal Atmos. Chem. Phys.
Discussion started: 10 September 2018

Atmospheric Chemistry and Physics Discussions

Relative Humidity Effect on the Formation of Highly Oxidized Molecules and New Particles during Monoterpene Oxidation

Xiaoxiao Li[1,2], Sabrina Chee[1], Jiming Hao[2], Jonathan P. D. Abbatt[3], Jingkun Jiang[2*], and James N. Smith[1*]

[1]Chemistry Department, University of California, Irvine, CA 92697, USA

[2]State Key Joint Laboratory of Environment Simulation and Pollution Control, School of Environment, Tsinghua University, Beijing, 100084, China

[3]Department of Chemistry, University of Toronto, Toronto, Canada

*: *Correspondence to*: J. N. Smith (jimsmith@uci.edu) and J. Jiang (jiangjk@tsinghua.edu.cn)

Abstract. It has been widely observed around the world that the frequency and intensity of new particle formation (NPF) events are reduced during periods of high relative humidity (RH). The current study focuses on how RH affects the formation of highly oxidized molecules (HOMs), which are key components of NPF and initial growth caused by oxidized organics. The ozonolysis of α-pinene, limonene, and Δ^3-carene, with and without OH-scavenger, were carried out under low NOx conditions under a range of RH (from ~3% to ~90%) in a temperature-controlled flow tube. A Scanning Mobility Particle Sizer (SMPS) was used to measure the size distribution of generated particles and a novel transverse-ionization chemical ionization inlet with a high-resolution time-of-fight mass spectrometer detected HOMs. A major finding from this work is that neither the detected HOMs nor their abundance changed significantly with RH, which indicates that the detected HOMs must be formed from water-independent pathways. In fact, the distinguished OH- and O_3-derived peroxy radicals (RO_2), HOM monomers, and HOM dimers could mostly be explained by the autoxidation of RO_2 followed by bimolecular reactions with other RO_2 or hydroperoxy radicals (HO_2), rather than from a water-influenced pathway like through the formation of a stabilized Criegee intermediate (sCI). However, as RH changed from 3 to 90% the particle number concentrations decreased by a factor of 2~3 while particle mass concentrations increased or decreased slightly within a factor of 2. These observations show that, while high RH appears to inhibit NPF as evident by the decreasing number concentration, this reduction is not caused by a decrease in RO_2-derived HOMs formation. One possible explanation is the existence of other extremely low volatility compounds (ELVOCs), like gas phase formed sCI-included accretion products, which are responsible for the very first steps of NPF but are not detected by nitrate-based chemical ionization mass spectrometry. These ELVOCs may be preferentially reduced at high RH compared to more volatile compounds, the latter of which mainly determine the final mass concentration of particles. Another possibility is that a fraction of HOMs cluster with water (but detected as the declustered molecules) at high RH in such a way that they may no longer be able to participate in cluster formation, thereby suppressing NPF.

Atmos. Chem. Phys. Discuss., https://doi.org/10.5194/acp-2018-898
Manuscript under review for journal Atmos. Chem. Phys.
Discussion started: 10 September 2018

Atmospheric Chemistry and Physics Discussions

1 Introduction

New particle formation (NPF) is ubiquitous around the world (Kulmala et al., 2004). Newly formed particles contribute greatly to global particle populations and can grow further to act as cloud condensation nuclei (CCN), thereby influencing clouds and climate (Makkonen et al., 2012; Merikanto et al., 2009; Dunne et al., 2016). NPF characteristics vary from site to site because of varying precursors and atmospheric conditions. It has been widely observed that the intensity (Sihto et al., 2006; Dada et al., 2017) and frequency (Dada et al., 2017; Boy and Kulmala, 2002; Hyvönen et al., 2005) of continental NPF are reduced during periods of high RH, resulting in reduced ultrafine particle number concentrations during these periods (Weber et al., 1997). For example, 20 years of observations in the boreal forest at Hyytiälä, Finland, showed that NPF is more likely during periods of low ambient RH (Dada et al., 2017). In central Amazonia, where particle composition is dominated by oxidation products of biogenic organic compounds, new particles were not formed at ground-level where RH was always higher than 60%, but rather formed in the upper troposphere where RH and condensation sink (CS) were significantly lower (Poschl et al., 2010; Andreae et al., 2018). In urban areas, NPF also favors low RH (Cai et al., 2017; Shen et al., 2011). Despite the low continental NPF event frequency at high RH, NPF has still been observed in the free troposphere in vicinity of clouds, where RH is extremely high (Weber et al., 1999) and in coastal and marine areas where RH is typically greater than 90% (O'Dowd et al., 1998).

The widely observed anti-correlation between NPF and RH in the field experiments can be attributed to the indirect influence of water. For example, high RH often corresponds to greater cloud cover, which can lead to lower ground-level concentrations of photo-oxidized precursors such as H_2SO_4 and highly oxidized molecules (HOMs) as well as an increased condensation sink that leads to scavenging of precursors and clusters (Hamed et al., 2011). On the other hand, water vapor may also directly influence NPF by regulating the formation of gas phase precursors or by participating in cluster formation. For example, chamber and model experiments on the binary sulfuric acid-water system have demonstrated positive relationships between particle formation rate and RH (Duplissy et al., 2016; Merikanto et al., 2016). While in the ternary (H_2SO_4/MSA-H_2O-Amine/NH_3) system, H_2O was reported to have either positive (Chen et al., 2015) or negative (Napari et al., 2002) effects on NPF. Some studies have hypothesized that high water content might suppress the formation of NPF-related organics from the oxidation of biogenic precursors (Hyvönen et al., 2005; Boy and Kulmala, 2002). However, no direct evidence of this has been provided.

Although sulfuric acid has been recognized as the most important precursor of new particle formation, it alone can't explain

the rapid formation and growth rates observed in the field (Kuang et al., 2008). Organic compounds, ammonia, amines, and water are also likely involved (Zhang et al., 2012; Chen et al., 2012). Organics have been shown to be very important for cluster formation and stabilization in theoretical studies (Ortega et al., 2016; Donahue et al., 2013), laboratory experiments (Tröstl et al., 2016; Schobesberger et al., 2013) and field measurements (Bianchi et al., 2016; Hoffmann et al., 2001; Metzger et al., 2010). Organics can either form clusters with sulfuric acid or purely with themselves (Zhao et al., 2013; Zhao et al., 2009). They can also contribute significantly to the condensational growth of newly formed particles, determining particle growth rates, particle lifetime, and global particle and CCN concentrations (Donahue et al., 2011; Vehkamäki and Riipinen, 2012). The ability of organics to take part in particle formation and condensational growth depends on their volatility as well as reactivity. HOMs, such as extremely low volatility organic compounds (ELVOCs, saturation mass concentration (C*) < 3×10^{-4} μg m^{-3}) or low volatility organic compounds (LVOCs, 3×10^{-4} < C* < 0.3 μg m^{-3}), are likely contributors to NPF (Donahue et al., 2012; Ehn et al., 2014).

Despite its large contribution to NPF, the direct measurement of HOMs has long been a challenge because of their low atmospheric concentrations, low volatilities, and short lifetimes. Recently, the development of the high resolution time-of-flight chemical ionization mass spectrometer (HRToF-CIMS) overcame this barrier and made the measurement and identification of HOMs feasible (Junninen et al., 2010; Jokinen et al., 2012). HOMs from both monoterpene and aromatic oxidation showed high O/C ratios of > 0.7-0.8, and were present as monomers, dimers and even higher order clusters (Molteni et al., 2018; Ehn et al., 2012). These high O/C ratios could not be explained by any of the formerly known oxidization pathways unless the autoxidation of RO_2 was taken into consideration (Crounse et al., 2013; Barsanti et al., 2017). Autoxidation was widely observed in condensed phase reactions, however, it was not considered in the gas phase previously because of the high energy barrier. This was further confirmed by the fact that at higher temperatures, more HOMs are formed than at low temperatures (Frege et al., 2018).

Since most laboratory experiments related to the formation of HOMs have been conducted under conditions of constant RH, usually low or medium RH of less than 60% (Ehn et al., 2012; Zhang et al., 2015), it was still unknown whether and how water vapor might impact HOMs formation. High RH conditions are difficult to achieve in chamber experiments without significantly changing temperature and pressure. In addition, HOMs detection by the current commercially available CIMS inlet based on the design of Eisele and Tanner is subject to water cluster influence (Kuerten et al., 2016).

In this research, three different endocyclic monoterpenes, α-pinene, limonene and Δ^3-carene were reacted with ozone, with

and without hydroxyl radical (OH) scavengers, in a reaction flow tube. RH influences on HOMs formation and organic-driven NPF were studied under a range of RH from 0% to 90%. Generated closed-shell HOMs and RO_2 were measured using a home-built CIMS inlet coupled to a HRToF mass spectrometer (LTOF mass analyzer, Tofwerk AG). The CIMS inlet effectively reduced water clustering onto ions sampled into vacuum, thus removing sample artifacts caused by high water vapor levels. Water vapor influence on the formation of RO_2, HOM monomers and HOM dimers were studied. The volatility of O_3- and OH-derived closed-shell HOMs were estimated with a group contribution-based model (SIMPOL) and a recently developed statistical model to study the potential contribution of O_3 and OH initiated chemistry on NPF.

2 Methods

2.1 Flow tube reactor

The experiments were performed in a laminar flow tube reactor consisting of a 150 cm long Pyrex glass cylinder with a volume of 8.5 dm^3 (Figure 1). The flow tube was located in a temperature controlled room (T=293±2°C) and was covered so that all experiments were performed under dark conditions. The monoterpenes were injected into the chamber using a syringe pump (model NE-300, New Era Pump Systems, Inc.) evaporated into a 2.5 LPM flow of dry, purified "zero air." O_3 was generated by passing 0.5 LPM dry zero air (79% N_2, 21% O_2) over a Hg UV lamp (model 90-0004-04, UVP, LLC) and then diluted with 6.5 LPM of zero air at the prescribed RH. The zero air was generated with a zero air generator (model 747-30, Aadco Instruments), with NOx and SO_2 concentrations specified to be less than 0.5 ppbv. Low NOx conditions were achieved using zero air as-is. A temperature-controlled bubbler filled with deionized water was used to generate humid air, and the prescribed RH was achieved by controlling the temperature of the bubbler. Gas inlets to the flow tube were made from Teflon tubing that were capped and drilled with small holes to distribute sample air uniformly in the flow tube cross section. The uniform distributions of O_3 and H_2O in the flow tube were confirmed by measuring [O_3] and RH at the different locations prior to the experiments. In every experiment, RH was adjusted to be constant for at least 30 min for each of the four RH steps (0~5%, 30~38%, 58~65%, 85~92%). The total flow rate was kept at 8.5 LPM so that the average reaction time was constant (~60s) for each experiment. At the beginning of the experiments, the inner wall of the reactor was washed with ultra-pure water. All of the flow rates were calibrated before and during the experiments.

2.2 Instrumentation

2.2.1 Transverse Ionization – Chemical Ionization Mass Spectrometer

A self-designed and home-built chemical ionization inlet, called Transverse Ionization (TI) inlet (Figure 2 and Figure S1), was used in front of the LTOF mass analyzer. The TI design is similar to those of the Ambient-pressure Proton transfer Mass Spectrometer (AmPMS) (Hanson et al., 2011) and the cluster-CIMS (Zhao et al., 2010). In the TI inlet, a 4-10 LPM flow of

sample air is passed across the inlet orifice of the mass spectrometer, where it encounters an orthogonal, 1 LPM reagent ion gas flow consisting N_2 containing ionized nitrate ions (NO_3^-) as well as potential cluster ions $(HNO_3)_nNO_3$ with n=1-3. For the current study, the sample flow to the inlet was set to 4.5 LPM. Chemical ionization occurs at atmospheric pressure and temperature. The reagent gas is generated by passing 3 ccm of N_2 over a small vial containing nitric acid, which is then ionized by a 370 MBq Po^{210} radioactive source (model P-2021, NRD, LLC). An additional flow of N_2 can be added to the reagent gas to change the reagent ion concentration, and the assembly can be adjusted to vary ion-molecule reaction time. The latter can be controlled by adjusting the sample and reagent gas flow rates or by applying different voltages to the ionization source and the main inlet block. To minimize the diffusion loss in sample lines, the inlet of the TI source was connected to the flow tube outlet by a short (~10 cm) piece of electro-polished stainless steel tubing. Compared to the widely used commercial nitrate source patterned after the design by Eisele and Tanner (1993) and marketed by Aerodyne, Inc., no additional sheath flow is required so thus any impurities potentially introduced by the sheath flow are eliminated. Some flow disturbance may occur where the sample flow encounters the transverse reagent flow, which may lead to non-ideal behavior. However, even at the maximum total flow of 11 LPM, the Reynolds number in this region is ~500 and thus turbulence is not expected to be significant.

Another unique aspect of the TI design is the use of an N_2 curtain gas in front of the inlet orifice to the mass spectrometer to reduce water clustering on reagent and sample ions. Water clusters are expected to form at high RH mainly during the free-jet expansion of the sampled gas on the vacuum side of the orifice plate (Thomson and Iribarne, 1979). The presence of these clusters makes the identification and quantification of both sample and reagent ions challenging (Kulmala et al., 2014; Lee et al., 2014; Kuerten et al., 2016; Ehn et al., 2014). Figure 2 shows the details of the TI source that address this issue. Small holes drilled in a radial channel blow N_2 uniformly in front of the orifice plate so that only sampled ions and this clean N_2 gas pass into the vacuum chamber. Since the sampling flow rate of the mass spectrometer is ~0.5 LPM when using 0.3 mm orifice, the N_2 curtain flow is set to be 1 LPM to overflow the region surrounding the orifice. By applying voltages to the ion source and the block, the ions can be efficiently guided into the mass spectrometer while neutral molecules such as water vapor are prevented from entering by the N_2 curtain gas.

This TI inlet is suitable to all types of reagent ion chemistry, e.g. NO_3^-, I^-, and H_3O^+. Nitrate ion chemistry was used as the reagent ion in these experiments, which is selective to highly oxidized molecules that have at least two hydroperoxy (-OOH) groups or some other H-bond-donating groups (Hyttinen et al., 2015). HOM monomers, HOM dimers and highly oxidized RO_2 radicals can also be measured using nitrate ion chemistry.

148

149 **2.2.2 Other measurements**

150 Ozone concentrations were measured with two ozone analyzers (model 106L, 2B Technology) at the inlet and outlet of the
151 flow tube. The sampling flow of each analyzer is 1 LPM. The two ozone analyzers were intercompared prior to the
152 experiments and the difference was within 5 ppbv when [O_3] < 1000 ppbv. A Scanning Mobility Particle Sizer (SMPS),
153 consisting of a Po210 bipolar neutralizer, a nano-Differential Mobility Analyzer (nano-DMA; model 3081, TSI, Inc.), and a
154 condensation particle counter (MCPC; model 1720, Brechtel Manufacturing) were used to measure the number-size
155 distribution of particles, which is later used to deduce the total particle number and mass concentrations (the latter assumes a
156 uniform density for organic particles of 1.2 g cm^{-3}). The sampling flow rate of the MCPC was 0.3 LPM and the sheath and
157 excess flows of the nano DMA were set to 3 LPM. The flow tube particle number-size distribution was measured without
158 further drying to get a more accurate measure of the actual particle surface area and volume, which are important for HOMs
159 partitioning, and also to prevent particle evaporation during the measurements.

160

161 **2.3 Experimental conditions**

162 Three monoterpenes were used in our experiments (see Table 1), α-pinene, limonene and Δ^3-carene. Oxidation by ozone is
163 believed to dominate over other oxidation radicals (i.e., OH or NO_3) in forming secondary organic aerosol (SOA) under
164 atmospheric conditions (Atkinson and Arey, 2003). Ozonolysis of alkenes generates a substantial amount of OH, leading to
165 products that are produced by a combination of O_3 and OH oxidation. For some experiments, in order to isolate oxidation by
166 O_3, cyclohexane (see Table 1 for mixing ratios) was premixed with the monoterpene and added to the flow tube as an OH
167 scavenger. For other experiments, the combination of OH and O_3 chemistry were investigated to study atmospheric oxidation
168 chemistry more representative of ambient air. The "high concentration" experiments were conducted with similar mixing
169 ratios of monoterpene (~1100ppb) and O_3 (~900ppb). The "low concentration" experiments were conducted to study the
170 particle-free chemical processes with initial concentrations of monoterpenes and O_3 shown in Table 1. Since wall losses
171 should be comparable for different precursors as a function of RH, it was not taken into consideration in our analysis of
172 HOMs production.

173

174 **2.4 HOMs volatility predictions**

175 The SIMPOL.1 method (Pankow and Asher, 2008) and the molecular corridor method (Li et al., 2016) were used to predict
176 the saturation mass concentrations (C*) of some of the detected OH- and O_3-related HOMs. SIMPOL.1 is a group
177 contribution method and requires information on molecular structure, while the molecular corridor method only requires the

molecular formulae. Both methods are semi-empirical and based on volatility data from hundreds or thousands of compounds. The calculated volatilities were then applied to the two-dimensional volatility basis set (2D-VBS) (Donahue et al., 2012) to explore the likelihood that the products participate in the initial stages of nanoparticle growth.

3 Results and discussion

3.1 TI-CIMS performance

When comparing the TI inlet with the commercial nitrate inlet in measuring α-pinene ozonolysis products, both inlets produced identical mass spectra. The sensitivities of both inlets to H_2SO_4 were determined using a home-built H_2SO_4 calibration system (Figure S2) based on the design of Kurten et al. (2012). Figure 3 summarizes the results of these calibrations. The position of the ion source relative to the inlet orifice is critical for determining the sensitivity of the TI inlet. When the ion source is placed 0.5 cm upstream along the sample flow axis and 5 cm away from the inlet orifice along the reagent ion flow axis (configuration shown in Figure 2), the instrument is at its most sensitive. The calibration factors, defined as $C = [H_2SO_4]/([HSO_4^-]/[NO_3^-])$ (Eisele and Tanner, 1993), for the TI in this position and the commercial inlet were 3.25×10^{10} molecules cm^{-3} and 1.41×10^{10} molecules cm^{-3}, respectively. The lower calibration factor for the TI is attributed to the shorter reaction time, which we estimate to be ~80 ms. The total ion count (TIC) of the TI inlet is more than 5 times higher than the commercial inlet, so the overall sensitivity is better. The lower detection limit for sulfuric acid, which is defined as three times the standard deviation of the background (Jokinen et al., 2012), is 9.3×10^4 molecules cm^{-3} and 1.26×10^5 molecules cm^{-3} for the TI and commercial inlet, respectively.

After applying the N_2 curtain gas flow, the TIC recorded by the TI-CIMS decreased significantly. This was compensated for by increasing the ion source and reaction chamber voltages that direct ions to the orifice (Figure S3). When RH>90%, the reagent ion mass spectrum was dominated by water clusters $(H_2O)_m(HNO_3)_nNO_3^-$ (m=0~30, n=0~2) if no N_2 curtain flow was applied. The reagent ions NO_3^-, $HNO_3NO_3^-$ and $(HNO_3)_2NO_3^-$ decreased as RH increased, with $[(HNO_3)_2NO_3^-]$ and $[HNO_3NO_3^-]$ decreasing much faster than $[NO_3^-]$. In contrast, after 1 LPM N_2 curtain flow was applied to the inlet, most of the water clusters were removed (Figure 4). The reagent ions, sample ions and TIC remained stable as RH increased, which resulted in a reliable measurement of HOMs concentrations as a function of RH. The result that the N_2 curtain flow eliminated water clustering to a large extent confirms that most of the water clusters in the spectrum were produced during the free-jet expansion into vacuum instead of formed in the ion-molecular reagent region.

Atmos. Chem. Phys. Discuss., https://doi.org/10.5194/acp-2018-898
Manuscript under review for journal Atmos. Chem. Phys.
Discussion started: 10 September 2018

Atmospheric Chemistry and Physics Discussions

3.2 Identification of HOMs spectrum

Figure 5 shows the average mass spectra of the HOMs dimers and Figure S4 shows the average mass spectra of the HOMs monomer and RO_2 radicals for each of the six particle generation experiments. More than 400 peaks were identified in each spectrum, the majority of which were clusters with NO_3^- or $HNO_3NO_3^-$. [H_2SO_4] was ~10^5 molecules cm^{-3} and was always less than 3% of the most abundant C_{10} products, suggesting that sulfuric acid plays a negligible role in nucleation and cluster growth in our experiments. After subtracting the reagent ions (NO_3^- or $HNO_3NO_3^-$), molecular formulae for organics with an odd number of H atoms were assigned to radicals, which are generally difficult to detect experimentally (Rissanen et al., 2015), and formulae with an even number of H atoms were assigned to closed-shell molecules. Most of the HOMs products from the three endocyclic monoterpenes were very similar, while the relative abundance of different HOMs was quite different, indicating similar reaction pathways but different branching ratios in the reaction mechanisms. The main products were $C_{5\text{-}10}H_{6\text{-}16}O_{3\text{-}10}$ for closed shell monomers and RO_2 and $C_{15\text{-}20}H_{22\text{-}34}O_{6\text{-}18}$ for closed shell dimers. Among these, C_{10} and C_{20} compounds were the most abundant. $C_{5\text{-}9}$ products could be formed from O_3 attack on the less reactive exocyclic carbon double bond or the decomposition of intermediate radicals. Some fragments were found to be unique for specific monoterpene precursors. For instance, $C_5H_6O_7$ (m/z 240) was much more abundant in α-pinene oxidation than from other two precursors, which might be a tri-carboxylic acid (Ehn et al., 2012).

Comparing total HOMs abundance for the three monoterpene oxidation reactions, limonene created the most, followed by α-pinene and then Δ^3-carene. This is in qualitative agreement with prior studies (Jokinen et al., 2014; Ehn et al., 2014). The total dimer signal intensity was 15-30% of monomers for all three monoterpenes. Experiments with an OH scavenger generated fewer HOMs than those without OH scavengers.

As observed in previous studies, $C_{10}H_{15}O_{6,8,10,12}$ and $C_{10}H_{17}O_{5,7,9,11}$ comprised the O_3- and OH-related RO_2, respectively (Jokinen et al., 2014), while $C_{10}H_{14}O_{5,7,9,11}$ and $C_{10}H_{16}O_{6,8,10,12}$ comprised the O_3- and OH-related closed shell monomers, respectively (Ehn et al., 2014). When comparing the average spectra with and without OH scavenger, no obvious differences were seen for OH-related RO_2 or monomers (Figure S4). In contrast, for dimers we found that $C_{20}H_{32}O_{6\text{-}13}$ were more abundant in experiments without OH scavenger (Figure 5). The formation of these dimers can be explained by the reaction of one OH-related RO_2 with one O_3-derived RO_2 (see Section 3.5), and can therefore be considered as markers for combined OH and O_3 chemistry. As HOMs dimers are generally less volatile than monomers with identical O/C ratio, rapid production of dimers is believed to play a more important role in initial particle formation and growth (Zhang et al., 2015).

3.3 RH influence on HOMs generation

Figure 6 shows a time series of experimental parameters, particle size distribution, and key ions from the limonene ozonolysis experiment with OH scavenger (EXP. 2 in Table 1). The O_3 inlet and outlet concentrations were approximately constant with increasing RH (Figure 6a), indicating that RH did not significantly change O_3 levels in the flow tube. This also shows that the reactivity of the limonene with ozone does not change with RH. The number concentration of the generated particles decreased from 4.9×10^6 cm^{-3} to 2.7×10^6 cm^{-3} with increasing RH, while the peak of the number-size distribution increased slightly, due in part to water absorption. When RH was above 80%, both the integrated number and mass concentrations, which were calculated from the number-size distributions, decreased (Figure 6b).

Despite the change in particle number and mass concentrations with RH, the concentration of all the main HOMs, including RO_2, monomers and dimers, did not change for both OH- and O_3-derived products (Figure 6c). In fact, the only signals in the mass spectra that changed with RH corresponded to an increases associated with water clusters. The variations in HOMs concentrations can be explained by the competition between production and condensational losses. With the changes of particle concentration, the condensation sink should also change with RH. However, in this experiment, as in all other experiments, the surface area for existing particles ($1.8\sim4.1\times10^{-6}$ m^2) was much lower than the wall surface area of the flow tube (~0.38 m^2). As almost all of the detected HOMs are ELVOCs or LVOCs (see Section 3.6), they are not likely to partition back to the gas phase after they encounter a wall. As a result, the main loss in the flow tube should be caused by wall loss, which does not change significantly with RH. To further test this hypothesis that wall losses dominated over condensation onto particles, particle free experiments were performed and, again, the detected HOMs signals did not change with RH (Figure 7).

3.4 RH influence on SOA generation

Figure 8 shows the integrated SOA particle number and mass concentrations. The generated SOA particle number and mass concentrations for limonene were ~5 times greater than for $\triangle^3$-carene and α-pinene. This is because the theoretical ozone reactivity of limonene is 3~5 times higher than the latter two and molar yield from limonene ozonolysis is also the highest. Peaks in the particle number-size distributions were between 40 and 70 nm (Figure S5). In most of the experiments, generated SOA mass concentrations increased or decreased slightly when RH increased from ~0% to ~60% and decreased as RH further increased to ~90%. The variability in particle mass concentration as a function of RH for different experiments can be attributed to combined effects of gas phase reactions, condensed phase reactions, as well as physical uptake of water, but all values were within a factor of two of each other. On the contrary, the particle number concentrations decreased by a

factor of 2~3 with increasing RH.

A number of studies have demonstrated different water and OH influences on the ozonolysis products of exocyclic and endocyclic organic compounds. They have reported either suppressing (Bonn et al., 2002; Bonn and Moorgat, 2002) or promoting (Jonsson et al., 2006; Jonsson et al., 2008) effects of water vapor on the particle formation processes during ozonolysis of monoterpenes by measuring the number-size distributions of generated SOA particles with SMPS. The discrepancies between different results could be attributed to the different experiment setups, e.g., monoterpene and O_3 concentration, temperature, RH range, OH scavengers, reaction time, and so on. Specifically, our results are in good agreement with those of Bonn et al., who studied SOA generation from the ozonolysis of endocyclic monoterpenes (Bonn et al., 2002). In that study, SOA number concentrations decreased by a factor of 1.1~2.5 as RH increased, while the variation in volume concentrations was negligible (within ±10%). They concluded that water's influence on non-volatile products, which are responsible for the initial steps of nucleation, was much larger than its influence for semi-volatile compounds which mainly determined the final volume concentrations of particles. Thus, it was highly suspected that water influenced new particle formation through influencing the generation of NPF precursors. However, our measurements indicate that at least the formation of the detected HOMs is independent of water vapor concentrations. There may be other species that are crucial to the initial steps of NPF and are affected by water vapor but are not detected by nitrate CIMS (see section 3.5). Another possible explanation is that a fraction of HOMs cluster with water at high RH in such a way that they may no longer be able to participate in further cluster formation, thereby suppressing NPF. If the CIMS measurement only detected the declustered molecule, then such a mechanism may still be consistent with our observations.

3.5 Possible water-relevant C_{10} and C_{20} HOMs formation pathways

Although the oxidation of BVOCs has been widely studied, it has mostly been constrained to the early stages (first and second generation intermediates) and many uncertainties still exist (Johnson and Marston, 2008; Isaacman-VanWertz et al., 2018; Atkinson and Arey, 2003). The first step of ozonolysis for the three BVOCs (α-pinene, $\triangle^3$-carene and limonene) is ozone attack on the endocyclic carbon double bond to form a primary ozonide. Figure 9 shows the O_3-initiated oxidation pathways of α-pinene that may be related to the detected C_{10} and C_{20} HOMs for representative isomers. The primary ozonide rapidly transforms to two excited Criegee intermediates (eCIs), one of which (branching ratio= 0.4) (Kamens et al., 1999) is shown in Figure 9. The reaction pathways of the eCI are complex, the most important two under ambient and most chamber conditions are the sCI channel (reaction I) and the hydroperoxide channel (reaction II) (Bonn et al., 2002). The sCI either reacts with aldehydes to form a secondary ozonide (when the aldehyde is C_{10}, then the formed SOZ is C_{20} and is marked as

297 sCI-C_{10}) or with water or other acidic compounds such as alcohols and carboxylic acids to form hydroxy-hydroperoxide,
298 which then decomposes to carboxylic acids or aldehydes. For α-pinene, the main decomposition product is pinonic acid. In
299 the hydroperoxide channel (reaction II), the formed hydroperoxide quickly decomposes to a first generation alkyl radical (R)
300 and OH (Johnson and Marston, 2008). R reacts with O_2 immediately to form the first generation RO_2, which can undergo
301 numerous reactions, including reaction with HO_2, $R'O_2$ and autoxidation. The reaction with HO_2 mainly forms
302 hydroperoxides, with a small fraction forming peroxides or carbonyl-containing compounds. However, the carbonyl cannot
303 be formed in most cases since the C atom bonded to O-O does not have available electrons for the carbonyl π-bond. When
304 reacted with another $R'O_2$, either ROOR' or an alkoxy radical (RO) or a carbonyl and a hydroperoxide are formed. The RO
305 can undergo isomerization, or form a carbonyl and HO_2, for which the branching ratios are extremely difficult to evaluate.
306 RO can also undergo decomposition, which is one of the pathways to form C_5~C_9. The autoxidation process is key to HOMs
307 formation. Each autoxidation step adds two O atoms to the molecule and thus increases the oxidation state very rapidly. The
308 competition between autoxidation processes and bimolecular reactions (RO_2 reactions with $R'O_2$ or HO_2) determines the
309 ultimate oxidation state of the products (Barsanti et al., 2017; Crounse et al., 2013; Rissanen et al., 2015).
310
311 OH can be generated in the ozonolysis of alkenes and the yield is near unity (Atkinson, 1997). The reaction of OH with
312 α-pinene directly forms first generation R and then RO_2; one possible structure for this RO_2 (branching ratio = 0.44), formed
313 from OH addition to the double bond (Berndt et al., 2016), is shown in Figure 9. However, the formed RO_2 ($C_{10}H_{17}O_{2m+1}$) are
314 not the same RO_2 as those formed through ozonolysis ($C_{10}H_{15}O_{2n+2}$) (McVay et al., 2016). Accordingly, the structure and
315 composition of C_{10} and C_{20} HOMs formed from OH or O_3 chemistry are different, and so too are their potential impacts on
316 NPF. The combined OH- and O_3-derived dimers ($C_{10}H_{32}O_{2(m+n)+3}$), formed by collision of an OH-derived RO_2 with an
317 O_3-derived RO_2, were only observed in ozonolysis experiments without OH scavenger.
318
319 The RO_2 autoxidation pathway explains most of the observed C_{10} and C_{20} compounds in the mass spectra. One exception to
320 this is that $C_{10}H_{18}O_{2m+1}$, $C_{10}H_{18}O_{2m}$ and $C_{20}H_{34}O_{2(m+m')}$ were not observed in the spectrum whereas in experiments performed
321 by Berndt et al., in which OH oxidation for α-pinene was studied, $C_{10}H_{18}O_{2m}$ and $C_{20}H_{34}O_{2(m+m')}$ dominated the mass
322 spectrum (Berndt et al., 2016). This could be explained by a low OH/O_3 ratio in our experiments, since unlike Berndt et al.
323 we did not provide a source of OH to the flow tube.
324
325 Despite this close agreement achieved by the RO_2 autoxidation mechanism and the observed mass spectra in our study, prior
326 studies suggest that other potential pathways cannot be excluded. An accretion product involving sCI is one possibility

(Barsanti et al., 2017). It is possible that sCI reacts with long-chain carboxylic acids or carbonyls, such as those with 10 carbon atoms, forming in this instance anhydrides (sCI-C_{10}, reaction IV) or secondary ozonides (sCI-C_{10}, reaction V) with vapor pressures lower than 10^{-15} torr (Kamens et al., 1999; Tobias and Ziemann, 2001; Bonn et al., 2002). The formation of anhydride is more likely in condensed phase, whereas there is also a possibility it can also happen in gas phase (Kamens et al., 1999). However, it is unknown whether these sCI-C_{10} can be detected using nitrate-CIMS as they may lack hydrogen bond donor moieties. The semi-volatile pinonic acid can also form HOMs after further oxidation by OH (Ehn et al., 2014), provided that excess α-pinene is not present to compete with pinonic acid for the generated OH.

Water vapor's influence on HOMs formation can be direct or indirect. For monoterpene oxidation, the direct participation of water vapor is to react with sCI, favoring the formation of the hydroperoxide and its decomposition products (reaction III) over the secondary ozonides (sCI-C_{10}, reaction IV) or possible anhydrides (sCI-C_{10}, reaction V). Since the formation of sCI-C_{10} is more likely to contribute to NPF than the products from sCI and water vapor (Kamens et al., 1999; Tobias et al., 2000), a decrease in low volatility sCI-C_{10} with high RH could explain the decreasing SOA number concentrations in our experiment. It has been shown previously that OH yields from the reactions of O_3 with a series of monoterpenes were not affected by the presence of water vapor (Atkinson et al., 1992; Aschmann et al., 2002), which implies that the hydroperoxide channel (reaction II) are similarly unaffected by water. Since the detected HOMs in our experiments were RH-independent, we conclude that all the detected HOMs were formed from hydroperoxide channel (reaction II) and not via the sCI channel (reaction I). Similarly, the detected HOMs were not likely to form through the hydration reaction (Equation 1) (Ehn et al., 2012), which is supposed to increase with increasing RH.

$$R - CHO + H_2O \rightarrow R - CH(OH)_2 \quad . \qquad \text{(Equation 1)}$$

The indirect water effect on HOMs formation includes the water influence on HO_2 fate. As water promotes HO_2 self-reaction (Equation 2), reaction of HO_2 with RO_2 should decrease and the related HOM monomers should likewise decrease with increasing RH. However, as the formation of both HOM monomers and dimers was not affected by H_2O, it was likely that water does not significantly increase HO_2 self-reaction or that HO_2 chemistry was not important in our experiments.

$$2HO_2 \xrightarrow{M,\, H_2O} H_2O_2 + O_2 \qquad \text{(Equation 2)}$$

3.6 Volatility predictions

The volatility of the gas phase products is one of the most important properties that determines whether a compound contributes to the formation, initial growth or further growth of SOA particles (Donahue et al., 2012; Kroll et al., 2011). As

the products with identical elemental composition can be formed from different bimolecular reactions of the intermediate RO_2, it is difficult to predict their exact structures. For the current study, the number of different structural and functional groups (e.g., aromatic rings, carbon double bonds, aldehydes, carbonyls, hydroxyls, ethers, hydroperoxyls) was estimated and used to derive saturation vapor pressure using SIMPOL.1 (Table S1). To simplify the calculation, the functional groups used here were directly predicted from the proposed formation pathways in Figure 10 and did not include intramolecular isomerization, although that may be important in some situations. For example, one of the ROOH can be replaced with an endo-peroxide via ring closure of unsaturated RO_2 (Berndt et al., 2016). To figure out the possible bias introduced by this simplification, the result was compared to those obtained using the Molecular Corridor method (Li et al., 2016), the latter of which does not require information on functional groups.

Figure 10 shows the predicted saturation mass concentrations, C*, of the main C_{10} and C_{20} closed shell products. The difference of C* predicted from the two methods was within one order of magnitude for C_{20} HOMs, and 3~4 orders of magnitude for C_{10} HOMs. The difference was due to the abundance of –OOH and –OH moieties, which contribute more to lowering saturation vapor pressures than other functional groups (Table S1). Despite these differences, nearly all of the C_{20} HOMs can be classified as ELVOCs, while C_{10} products were mostly LVOCs. Typically, the volatilities of O_3-derived C_{20} HOMs were less than OH-related HOMs, whereas for those with identical oxidation states of carbon, $\overline{OSc}$ (defined as 2O/C-H/C) (Kroll et al., 2011), such as $C_{20}H_{30}O_{10}$ (O_3-derived dimer), $C_{20}H_{32}O_{11}$ (OH and O_3 combined dimer), $C_{20}H_{34}O_{12}$ (OH-derived dimer), OH-derived C_{20} HOMs have lower volatilities than O_3-derived HOMs due to a greater number of oxygen atoms in the former.

4 Conclusions

The RH influence on HOMs formation and NPF during monoterpene oxidation was explored in this study. HOMs were detected with a TI-CIMS, using nitrate as reagent ions; C_{10} and C_{20} dominated the spectra. There are mainly three potential paths for water vapor influence on the formation of C_{10} and C_{20} HOMs. One is water reacting with sCI (Equation 1), thereby influencing the branching ratio between formation of more volatile compounds decomposed from hydroxyl hydroperoxide, such as pinonic acid, and accretion products with sCI such as secondary ozonide (sCI-C_{10}) and anhydride (sCI-C_{10}). The second hypothesized water influence is on the HOMs formed from hydration reactions (Equation 2). The third is that water increases the rate of self-reaction of HO_2 (Equation 3), thus indirectly impacts the loss pathways of RO_2. Our experimental results, both with high particle loading and particle-free conditions, demonstrated that neither the detected HOMs species nor their signal abundance changed significantly with RH. This indicates that the detected HOMs, which can mostly be

explained by RO_2 autoxidation, must be formed from water-independent pathways rather than by those reactions mentioned above. One implication of this result is that HO_2 self-reaction was not significantly promoted by water or that the RO_2 reaction with HO_2 was not be significant in our system, but instead that RO_2 reacts with another peroxy radical, $R'O_2$, to generate both closed shell monomers and dimers. Another implication is that the sCI pathway is not responsible for the generation of the detected HOMs while the role of sCI-related HOMs (SOZ or anhydride) formation by accretion with long chain products, which may not be detected with nitrate CIMS, may be important in causing the decrease in SOA number concentrations with increased RH. Another possible explanation for the decreasing SOA number concentration is that water may cluster with HOMs and suppress NPF.

The detected HOMs, which could mostly be explained by autoxidation of RO_2 followed by reactions with $R'O_2$ or HO_2, were distinguished as OH-related, O_3-related RO_2, closed shell HOM monomers, and HOM dimers. The volatility of the identified products were estimated with the SIMPOL.1 group contribution method and with the molecular corridor technique. That analysis confirmed that C_{20} closed shell products have significantly lower volatility compared to C_{10} products and are thus more likely to contribute to NPF. Pure O_3 chemistry produced lower volatility C_{20} closed shell products compared to processes that were influenced or dominated by OH. As a result, O_3 chemistry is suspected to be more likely to lead to NPF than OH chemistry, given the same level of oxidants and VOCs precursors.

Acknowledgements

This research was supported by the US Department of Energy's Atmospheric System Research program under grant no. DESC0014469, the US National Science Foundation under grant no. AGS-1762098, and by the National Key R&D Program of China under grant no. 2017YFC0209503. XL thanks the financial support from the State Scholarship Fund managed by Chinese Scholarship Council (CSC). We thank Hayley Glicker, Deanna Caroline Myers, Michael Lawler, and Danielle Draper for their kind help.

References

Andreae, M. O., Afchine, A., Albrecht, R., Holanda, B. A., Artaxo, P., Barbosa, H. M., Borrmann, S., Cecchini, M. A., Costa, A., and Dollner, M.: Aerosol characteristics and particle production in the upper troposphere over the Amazon Basin, Atmos Chem Phys, 18, 921-961, 2018.

Aschmann, S. M., Arey, J., and Atkinson, R.: OH radical formation from the gas-phase reactions of O-3 with a series of

terpenes, Atmos Environ, 36, 4347-4355, 10.1016/s1352-2310(02)00355-2, 2002.
Atkinson, R., Aschmann, S. M., Arey, J., and Shorees, B.: Formation of OH radicals in the gas phase reactions of O3 with a series of terpenes, Journal of Geophysical Research: Atmospheres, 97, 6065-6073, 1992.
Atkinson, R.: Gas-phase tropospheric chemistry of volatile organic compounds: 1. Alkanes and alkenes, Journal of Physical and Chemical Reference Data, 26, 215-290, 1997.
Atkinson, R., and Arey, J.: Gas-phase tropospheric chemistry of biogenic volatile organic compounds: a review, Atmos Environ, 37, 197-219, 2003.
Barsanti, K. C., Kroll, J. H., and Thornton, J. A.: Formation of Low-Volatility Organic Compounds in the Atmosphere: Recent Advancements and Insights, Journal of Physical Chemistry Letters, 8, 1503-1511, 10.1021/acs.jpclett.7b02969, 2017.
Berndt, T., Richters, S., Jokinen, T., Hyttinen, N., Kurtén, T., Otkjær, R. V., Kjaergaard, H. G., Stratmann, F., Herrmann, H., and Sipilä, M.: Hydroxyl radical-induced formation of highly oxidized organic compounds, Nature communications, 7, 13677, 2016.
Bianchi, F., Tröstl, J., Junninen, H., Frege, C., Henne, S., Hoyle, C. R., Molteni, U., Herrmann, E., Adamov, A., and Bukowiecki, N.: New particle formation in the free troposphere: A question of chemistry and timing, Science, aad5456, 2016.
Bonn, B., and Moorgat, G.: New particle formation during a-and b-pinene oxidation by O 3, OH and NO 3, and the influence of water vapour: particle size distribution studies, Atmos Chem Phys, 2, 183-196, 2002.
Bonn, B., Schuster, G., and Moortgat, G. K.: Influence of water vapor on the process of new particle formation during monoterpene ozonolysis, The Journal of Physical Chemistry A, 106, 2869-2881, 2002.
Boy, M., and Kulmala, M.: Nucleation events in the continental boundary layer: Influence of physical and meteorological parameters, Atmos Chem Phys, 2, 1-16, 2002.
Cai, R., Yang, D., Fu, Y., Wang, X., Li, X., Ma, Y., Hao, J., Zheng, J., and Jiang, J.: Aerosol surface area concentration: a governing factor in new particle formation in Beijing, Atmos Chem Phys, 17, 12327, 2017.
Chen, H., Ezell, M. J., Arquero, K. D., Varner, M. E., Dawson, M. L., Gerber, R. B., and Finlayson-Pitts, B. J.: New particle formation and growth from methanesulfonic acid, trimethylamine and water, Physical Chemistry Chemical Physics, 17, 13699-13709, 2015.
Chen, M., Titcombe, M., Jiang, J., Jen, C., Kuang, C., Fischer, M. L., Eisele, F. L., Siepmann, J. I., Hanson, D. R., and Zhao, J.: Acid–base chemical reaction model for nucleation rates in the polluted atmospheric boundary layer, Proceedings of the National Academy of Sciences, 109, 18713-18718, 2012.
Crounse, J. D., Nielsen, L. B., Jørgensen, S., Kjaergaard, H. G., and Wennberg, P. O.: Autoxidation of organic compounds in the atmosphere, The Journal of Physical Chemistry Letters, 4, 3513-3520, 2013.
Dada, L., Paasonen, P., Nieminen, T., Buenrostro Mazon, S., Kontkanen, J., Peräkylä, O., Lehtipalo, K., Hussein, T., Petäjä, T., and Kerminen, V.-M.: Long-term analysis of clear-sky new particle formation events and nonevents in Hyytiälä, Atmos Chem Phys, 17, 6227-6241, 2017.
Donahue, N. M., Trump, E. R., Pierce, J. R., and Riipinen, I.: Theoretical constraints on pure vapor-pressure driven condensation of organics to ultrafine particles, Geophys Res Lett, 38, 10.1029/2011gl048115, 2011.
Donahue, N. M., Kroll, J., Pandis, S. N., and Robinson, A. L.: A two-dimensional volatility basis set–Part 2: Diagnostics of organic-aerosol evolution, Atmos Chem Phys, 12, 615-634, 2012.
Donahue, N. M., Ortega, I. K., Chuang, W., Riipinen, I., Riccobono, F., Schobesberger, S., Dommen, J., Baltensperger, U., Kulmala, M., Worsnop, D. R., and Vehkamaki, H.: How do organic vapors contribute to new-particle formation?, Faraday discussions, 165, 91-104, 10.1039/c3fd00046j, 2013.
Dunne, E. M., Gordon, H., Kuerten, A., Almeida, J., Duplissy, J., Williamson, C., Ortega, I. K., Pringle, K. J., Adamov, A., Baltensperger, U., Barmet, P., Benduhn, F., Bianchi, F., Breitenlechner, M., Clarke, A., Curtius, J., Dommen, J., Donahue, N. M., Ehrhart, S., Flagan, R. C., Franchin, A., Guida, R., Hakala, J., Hansel, A., Heinritzi, M., Jokinen, T., Kangasluoma, J., Kirkby, J., Kulmala, M., Kupc, A., Lawler, M. J., Lehtipalo, K., Makhmutov, V., Mann, G., Mathot, S., Merikanto, J.,

460 Miettinen, P., Nenes, A., Onnela, A., Rap, A., Reddington, C. L. S., Riccobono, F., Richards, N. A. D., Rissanen, M. P.,
461 Rondo, L., Sarnela, N., Schobesberger, S., Sengupta, K., Simon, M., Sipila, M., Smith, J. N., Stozkhov, Y., Tome, A., Trostl,
462 J., Wagner, P. E., Wimmer, D., Winkler, P. M., Worsnop, D. R., and Carslaw, K. S.: Global atmospheric particle formation
463 from CERN CLOUD measurements, Science, 354, 1119-1124, 10.1126/science.aaf2649, 2016.
464 Duplissy, J., Merikanto, J., Franchin, A., Tsagkogeorgas, G., Kangasluoma, J., Wimmer, D., Vuollekoski, H., Schobesberger,
465 S., Lehtipalo, K., and Flagan, R.: Effect of ions on sulfuric acid - water binary particle formation: 2. Experimental data and
466 comparison with QC - normalized classical nucleation theory, Journal of Geophysical Research: Atmospheres, 121,
467 1752-1775, 2016.
468 Ehn, M., Kleist, E., Junninen, H., Petäjä, T., Lönn, G., Schobesberger, S., Maso, M. D., Trimborn, A., Kulmala, M., and
469 Worsnop, D.: Gas phase formation of extremely oxidized pinene reaction products in chamber and ambient air, Atmos Chem
470 Phys, 12, 5113-5127, 2012.
471 Ehn, M., Thornton, J. A., Kleist, E., Sipila, M., Junninen, H., Pullinen, I., Springer, M., Rubach, F., Tillmann, R., Lee, B.,
472 Lopez-Hilfiker, F., Andres, S., Acir, I.-H., Rissanen, M., Jokinen, T., Schobesberger, S., Kangasluoma, J., Kontkanen, J.,
473 Nieminen, T., Kurten, T., Nielsen, L. B., Jorgensen, S., Kjaergaard, H. G., Canagaratna, M., Dal Maso, M., Berndt, T., Petaja,
474 T., Wahner, A., Kerminen, V.-M., Kulmala, M., Worsnop, D. R., Wildt, J., and Mentel, T. F.: A large source of low-volatility
475 secondary organic aerosol, Nature, 506, 476-+, 10.1038/nature13032, 2014.
476 Eisele, F. L., and Tanner, D. J.: Measurement of the gas-phas concentration of H2SO4 and methane sulfonic-acid and
477 estimates of H2SO4 production and loss in the atmosphere, J Geophys Res-Atmos, 98, 9001-9010, 10.1029/93jd00031,
478 1993.
479 Frege, C., Ortega, I. K., Rissanen, M. P., Praplan, A. P., Steiner, G., Heinritzi, M., Ahonen, L., Amorim, A., Bernhammer,
480 A.-K., and Bianchi, F.: Influence of temperature on the molecular composition of ions and charged clusters during pure
481 biogenic nucleation, Atmos Chem Phys, 18, 65-79, 2018.
482 Hamed, A., Korhonen, H., Sihto, S. L., Joutsensaari, J., Järvinen, H., Petäjä, T., Arnold, F., Nieminen, T., Kulmala, M., and
483 Smith, J. N.: The role of relative humidity in continental new particle formation, Journal of Geophysical Research:
484 Atmospheres, 116, 2011.
485 Hanson, D., McMurry, P., Jiang, J., Tanner, D., and Huey, L.: Ambient pressure proton transfer mass spectrometry: detection
486 of amines and ammonia, Environ Sci Technol, 45, 8881-8888, 2011.
487 Hoffmann, T., O'Dowd, C. D., and Seinfeld, J. H.: Iodine oxide homogeneous nucleation: An explanation for coastal new
488 particle production, Geophys Res Lett, 28, 1949-1952, 2001.
489 Hyttinen, N., Kupiainen-Määttä, O., Rissanen, M. P., Muuronen, M., Ehn, M., and Kurtén, T.: Modeling the charging of
490 highly oxidized cyclohexene ozonolysis products using nitrate-based chemical ionization, The Journal of Physical Chemistry
491 A, 119, 6339-6345, 2015.
492 Hyvönen, S., Junninen, H., Laakso, L., Maso, M. D., Grönholm, T., Bonn, B., Keronen, P., Aalto, P., Hiltunen, V., and Pohja,
493 T.: A look at aerosol formation using data mining techniques, Atmos Chem Phys, 5, 3345-3356, 2005.
494 Isaacman-VanWertz, G., Massoli, P., O'Brien, R., Lim, C., Franklin, J. P., Moss, J. A., Hunter, J. F., Nowak, J. B.,
495 Canagaratna, M. R., and Misztal, P. K.: Chemical evolution of atmospheric organic carbon over multiple generations of
496 oxidation, Nature chemistry, 1, 2018.
497 Johnson, D., and Marston, G.: The gas-phase ozonolysis of unsaturated volatile organic compounds in the troposphere,
498 Chemical Society Reviews, 37, 699-716, 2008.
499 Jokinen, T., Sipila, M., Junninen, H., Ehn, M., Lonn, G., Hakala, J., Petaja, T., Mauldin, R. L., Kulmala, M., and Worsnop, D.
500 R.: Atmospheric sulphuric acid and neutral cluster measurements using CI-APi-TOF, Atmos Chem Phys, 12, 4117-4125,
501 2012.
502 Jokinen, T., Sipilä, M., Richters, S., Kerminen, V. M., Paasonen, P., Stratmann, F., Worsnop, D., Kulmala, M., Ehn, M., and
503 Herrmann, H.: Rapid autoxidation forms highly oxidized RO2 radicals in the atmosphere, Angewandte Chemie International
504 Edition, 53, 14596-14600, 2014.

505 Jonsson, Å. M., Hallquist, M., and Ljungström, E.: Impact of humidity on the ozone initiated oxidation of limonene,
506 Δ3-carene, and α-pinene, Environ Sci Technol, 40, 188-194, 2006.
507 Jonsson, Å. M., Hallquist, M., and Ljungström, E.: Influence of OH scavenger on the water effect on secondary organic
508 aerosol formation from ozonolysis of limonene, Δ3-carene, and α-pinene, Environ Sci Technol, 42, 5938-5944, 2008.
509 Junninen, H., Ehn, M., Petaja, T., Luosujarvi, L., Kotiaho, T., Kostiainen, R., Rohner, U., Gonin, M., Fuhrer, K., Kulmala,
510 M., and Worsnop, D. R.: A high-resolution mass spectrometer to measure atmospheric ion composition, Atmos Meas Tech, 3,
511 1039-1053, 2010.
512 Kamens, R., Jang, M., Chien, C.-J., and Leach, K.: Aerosol Formation from the Reaction of α-Pinene and Ozone Using a
513 Gas-Phase Kinetics-Aerosol Partitioning Model, Environ Sci Technol, 33, 1430-1438, 10.1021/es980725r, 1999.
514 Kroll, J. H., Donahue, N. M., Jimenez, J. L., Kessler, S. H., Canagaratna, M. R., Wilson, K. R., Altieri, K. E., Mazzoleni, L.
515 R., Wozniak, A. S., Bluhm, H., Mysak, E. R., Smith, J. D., Kolb, C. E., and Worsnop, D. R.: Carbon oxidation state as a
516 metric for describing the chemistry of atmospheric organic aerosol, Nature Chemistry, 3, 133-139, 10.1038/nchem.948,
517 2011.
518 Kuang, C., McMurry, P. H., McCormick, A. V., and Eisele, F. L.: Dependence of nucleation rates on sulfuric acid vapor
519 concentration in diverse atmospheric locations, J Geophys Res, 113, 10.1029/2007jd009253, 2008.
520 Kuerten, A., Bergen, A., Heinritzi, M., Leiminger, M., Lorenz, V., Piel, F., Simon, M., Sitals, R., Wagner, A. C., and Curtius,
521 J.: Observation of new particle formation and measurement of sulfuric acid, ammonia, amines and highly oxidized organic
522 molecules at a rural site in central Germany, Atmos Chem Phys, 16, 12793-12813, 10.5194/acp-16-12793-2016, 2016.
523 Kulmala, M., Vehkamäki, H., Petäjä, T., Dal Maso, M., Lauri, A., Kerminen, V. M., Birmili, W., and McMurry, P. H.:
524 Formation and growth rates of ultrafine atmospheric particles: a review of observations, J Aerosol Sci, 35, 143-176,
525 10.1016/j.jaerosci.2003.10.003, 2004.
526 Kulmala, M., Petäjä, T., Ehn, M., Thornton, J., Sipilä, M., Worsnop, D., and Kerminen, V.-M.: Chemistry of atmospheric
527 nucleation: on the recent advances on precursor characterization and atmospheric cluster composition in connection with
528 atmospheric new particle formation, Annual review of physical chemistry, 65, 21-37, 2014.
529 Kurten, A., Rondo, L., Ehrhart, S., and Curtius, J.: Calibration of a Chemical Ionization Mass Spectrometer for the
530 Measurement of Gaseous Sulfuric Acid, J Phys Chem A, 116, 6375-6386, 2012.
531 Lee, B. H., Lopez-Hilfiker, F. D., Mohr, C., Kurtén, T., Worsnop, D. R., and Thornton, J. A.: An iodide-adduct
532 high-resolution time-of-flight chemical-ionization mass spectrometer: Application to atmospheric inorganic and organic
533 compounds, Environ Sci Technol, 48, 6309-6317, 2014.
534 Li, Y., Poeschl, U., and Shiraiwa, M.: Molecular corridors and parameterizations of volatility in the chemical evolution of
535 organic aerosols, Atmos Chem Phys, 16, 3327-3344, 10.5194/acp-16-3327-2016, 2016.
536 Makkonen, R., Asmi, A., Kerminen, V. M., Boy, M., Arneth, A., Hari, P., and Kulmala, M.: Air pollution control and
537 decreasing new particle formation lead to strong climate warming, Atmos Chem Phys, 12, 1515-1524,
538 10.5194/acp-12-1515-2012, 2012.
539 McVay, R. C., Zhang, X., Aumont, B., Valorso, R., Camredon, M., La, Y. S., Wennberg, P. O., and Seinfeld, J. H.: SOA
540 formation from the photooxidation of α-pinene: systematic exploration of the simulation of chamber data, Atmos Chem Phys,
541 16, 2785-2802, 2016.
542 Merikanto, J., Spracklen, D., Mann, G., Pickering, S., and Carslaw, K.: Impact of nucleation on global CCN, Atmos Chem
543 Phys, 9, 8601-8616, 2009.
544 Merikanto, J., Duplissy, J., Määttänen, A., Henschel, H., Donahue, N. M., Brus, D., Schobesberger, S., Kulmala, M., and
545 Vehkamäki, H.: Effect of ions on sulfuric acid - water binary particle formation: 1. Theory for kinetic - and nucleation -
546 type particle formation and atmospheric implications, Journal of Geophysical Research: Atmospheres, 121, 1736-1751,
547 2016.
548 Metzger, A., Verheggen, B., Dommen, J., Duplissy, J., Prevot, A. S., Weingartner, E., Riipinen, I., Kulmala, M., Spracklen, D.
549 V., Carslaw, K. S., and Baltensperger, U.: Evidence for the role of organics in aerosol particle formation under atmospheric

conditions, Proc Natl Acad Sci U S A, 107, 6646-6651, 10.1073/pnas.0911330107, 2010.
Molteni, U., Bianchi, F., Klein, F., Haddad, I. E., Frege, C., Rossi, M. J., Dommen, J., and Baltensperger, U.: Formation of highly oxygenated organic molecules from aromatic compounds, Atmos Chem Phys, 18, 1909-1921, 2018.
Napari, I., Noppel, M., Vehkamäki, H., and Kulmala, M.: Parametrization of ternary nucleation rates for H2SO4 - NH3 - H2O vapors, Journal of Geophysical Research: Atmospheres, 107, 2002.
O'Dowd, C. D., Geever, M., Hill, M. K., Smith, M. H., and Jennings, S. G.: New particle formation: Nucleation rates and spatial scales in the clean marine coastal environment, Geophys Res Lett, 25, 1661-1664, 1998.
Ortega, I. K., Donahue, N. M., Kurten, T., Kulmala, M., Focsa, C., and Vehkamaki, H.: Can Highly Oxidized Organics Contribute to Atmospheric New Particle Formation?, J Phys Chem A, 120, 1452-1458, 10.1021/acs.jpca.5b07427, 2016.
Pankow, J. F., and Asher, W. E.: SIMPOL. 1: a simple group contribution method for predicting vapor pressures and enthalpies of vaporization of multifunctional organic compounds, Atmos Chem Phys, 8, 2773-2796, 2008.
Poschl, U., Martin, S. T., Sinha, B., Chen, Q., Gunthe, S. S., Huffman, J. A., Borrmann, S., Farmer, D. K., Garland, R. M., Helas, G., Jimenez, J. L., King, S. M., Manzi, A., Mikhailov, E., Pauliquevis, T., Petters, M. D., Prenni, A. J., Roldin, P., Rose, D., Schneider, J., Su, H., Zorn, S. R., Artaxo, P., and Andreae, M. O.: Rainforest Aerosols as Biogenic Nuclei of Clouds and Precipitation in the Amazon, Science, 329, 1513-1516, 2010.
Rissanen, M. P., Kurtén, T., Sipilä, M., Thornton, J. A., Kausiala, O., Garmash, O., Kjaergaard, H. G., Petäjä, T., Worsnop, D. R., and Ehn, M.: Effects of chemical complexity on the autoxidation mechanisms of endocyclic alkene ozonolysis products: From methylcyclohexenes toward understanding α-pinene, The Journal of Physical Chemistry A, 119, 4633-4650, 2015.
Schobesberger, S., Junninen, H., Bianchi, F., Lonn, G., Ehn, M., Lehtipalo, K., Dommen, J., Ehrhart, S., Ortega, I. K., Franchin, A., Nieminen, T., Riccobono, F., Hutterli, M., Duplissy, J., Almeida, J., Amorim, A., Breitenlechner, M., Downard, A. J., Dunne, E. M., Flagan, R. C., Kajos, M., Keskinen, H., Kirkby, J., Kupc, A., Kurten, A., Kurten, T., Laaksonen, A., Mathot, S., Onnela, A., Praplan, A. P., Rondo, L., Santos, F. D., Schallhart, S., Schnitzhofer, R., Sipila, M., Tome, A., Tsagkogeorgas, G., Vehkamaki, H., Wimmer, D., Baltensperger, U., Carslaw, K. S., Curtius, J., Hansel, A., Petaja, T., Kulmala, M., Donahue, N. M., and Worsnop, D. R.: Molecular understanding of atmospheric particle formation from sulfuric acid and large oxidized organic molecules, Proc Natl Acad Sci U S A, 110, 17223-17228, 10.1073/pnas.1306973110, 2013.
Shen, X. J., Sun, J. Y., Zhang, Y. M., Wehner, B., Nowak, A., Tuch, T., Zhang, X. C., Wang, T. T., Zhou, H. G., Zhang, X. L., Dong, F., Birmili, W., and Wiedensohler, A.: First long-term study of particle number size distributions and new particle formation events of regional aerosol in the North China Plain, Atmos Chem Phys, 11, 1565-1580, 10.5194/acp-11-1565-2011, 2011.
Sihto, S.-L., Kulmala, M., Kerminen, V.-M., Maso, M. D., Petäjä, T., Riipinen, I., Korhonen, H., Arnold, F., Janson, R., and Boy, M.: Atmospheric sulphuric acid and aerosol formation: implications from atmospheric measurements for nucleation and early growth mechanisms, Atmos Chem Phys, 6, 4079-4091, 2006.
Thomson, B., and Iribarne, J.: Field induced ion evaporation from liquid surfaces at atmospheric pressure, The Journal of Chemical Physics, 71, 4451-4463, 1979.
Tobias, H. J., Docherty, K. S., Beving, D. E., and Ziemann, P. J.: Effect of relative humidity on the chemical composition of secondary organic aerosol formed from reactions of 1-tetradecene and O3, Environ Sci Technol, 34, 2116-2125, 2000.
Tobias, H. J., and Ziemann, P. J.: Kinetics of the gas-phase reactions of alcohols, aldehydes, carboxylic acids, and water with the C13 stabilized Criegee intermediate formed from ozonolysis of 1-tetradecene, The Journal of Physical Chemistry A, 105, 6129-6135, 2001.
Tröstl, J., Chuang, W. K., Gordon, H., Heinritzi, M., Yan, C., Molteni, U., Ahlm, L., Frege, C., Bianchi, F., and Wagner, R.: The role of low-volatility organic compounds in initial particle growth in the atmosphere, Nature, 533, 527-531, 2016.
Vehkamäki, H., and Riipinen, I.: Thermodynamics and kinetics of atmospheric aerosol particle formation and growth, Chemical Society Reviews, 41, 5160-5173, 2012.
Weber, R., Marti, J., McMurry, P., Eisele, F., Tanner, D., and Jefferson, A.: Measurements of new particle formation and ultrafine particle growth rates at a clean continental site, Journal of Geophysical Research: Atmospheres, 102, 4375-4385,

595 1997.
596 Weber, R., McMurry, P. H., Mauldin, R., Tanner, D., Eisele, F., Clarke, A., and Kapustin, V.: New particle formation in the
597 remote troposphere: A comparison of observations at various sites, Geophys Res Lett, 26, 307-310, 1999.
598 Zhang, R., Khalizov, A., Wang, L., Hu, M., and Xu, W.: Nucleation and growth of nanoparticles in the atmosphere, Chem
599 Rev, 112, 1957-2011, 10.1021/cr2001756, 2012.
600 Zhang, X., McVay, R. C., Huang, D. D., Dalleska, N. F., Aumont, B., Flagan, R. C., and Seinfeld, J. H.: Formation and
601 evolution of molecular products in α-pinene secondary organic aerosol, Proceedings of the National Academy of Sciences,
602 112, 14168-14173, 2015.
603 Zhao, J., Khalizov, A., Zhang, R., and McGraw, R.: Hydrogen-bonding interaction in molecular complexes and clusters of
604 aerosol nucleation precursors, The Journal of Physical Chemistry A, 113, 680-689, 2009.
605 Zhao, J., Eisele, F. L., Titcombe, M., Kuang, C., and McMurry, P. H.: Chemical ionization mass spectrometric measurements
606 of atmospheric neutral clusters using the cluster - CIMS, Journal of Geophysical Research: Atmospheres, 115, 2010.
607 Zhao, J., Ortega, J., Chen, M., and Mcmurry, P. H.: Dependence of particle nucleation and growth on high molecular weight
608 gas phase products during ozonolysis of α-pinene, Atmospheric Chemistry & Physics, 13, 7631-7644, 2013.
609

Atmos. Chem. Phys. Discuss., https://doi.org/10.5194/acp-2018-898
Manuscript under review for journal Atmos. Chem. Phys.
Discussion started: 10 September 2018

Atmospheric Chemistry and Physics Discussions

Table 1. Experiment conditions and products.

Precursor	Exp (#)	Monoterpene (ppbv)	O_3 (ppbv)	Cyclo-hexane (ppmv)	Initial rate[1] (10^8 molecules cm^{-3} s^{-1})	O_3 consumption[2] (ppb)	SOA[3] ($\mu g\ m^{-3}$)
Limonene	1	1085	900±10	0	1410	159-166	138-208
	2	1085	900±10	217	1410	139-150	81-147
	3	54	350±5	0	27.3	34-41	0
α-pinene	4	1111	900±10	0	625	103-110	761-1042
	5	1111	900±10	222	625	93-102	414-735
	6	54	350±5	0	11.8	23-30	0
Δ^3-carene	7	1111	900±10	0	267	72-89	55-93
	8	1111	900±10	222	267	70-86	34-92
	9	54	350±5	0	5.05	11-16	0

[1]At room temperature (298K), the rate coefficients for limonene, α-pinene and Δ^3-carene to react with O_3 were 200×10^{-18}, 86.6×10^{-18}, 37×10^{-18} cm^3 $molecule^{-1}$ s^{-1}, respectively.

[2]O_3 consumption values were calculated from the difference between inlet and outlet O_3 concentrations.

[3]SOA mass concentrations were calculated from SMPS-measured volume concentrations and an assumed organic effective density ($1.2\ g\ cm^{-3}$).

Atmos. Chem. Phys. Discuss., https://doi.org/10.5194/acp-2018-898
Manuscript under review for journal Atmos. Chem. Phys.
Discussion started: 10 September 2018

Atmospheric Chemistry and Physics Discussions

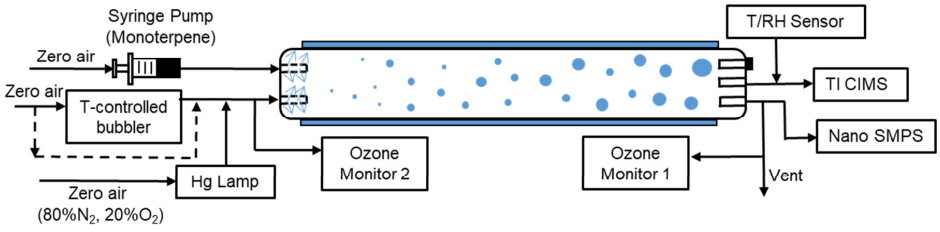

617

618 **Figure 1. Experiment setup for the flow tube experiments. The 8.5 L flow tube was placed at a temperature-controlled room**
619 **(21±1°C) and covered. The total flowrate was 8.5 LPM. The RH was adjusted by mixing temperature controlled bubbler flow with**
620 **dry zero air.**

621

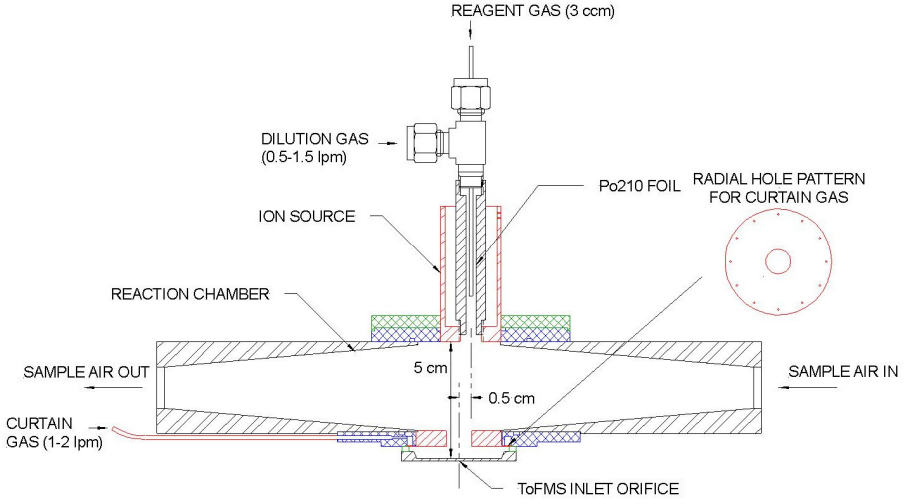

622

623 **Figure 2. Schematic of the transverse ionization (TI) inlet, showing the N_2 curtain gas configuration. The relative position of the**
624 **ion source to the inlet orifice is adjustable. The configuration shown here is the most sensitive in calibrations with H_2SO_4 (see**
625 **Section 3.1).**

626

Atmos. Chem. Phys. Discuss., https://doi.org/10.5194/acp-2018-898
Manuscript under review for journal Atmos. Chem. Phys.
Discussion started: 10 September 2018

Atmospheric Chemistry and Physics Discussions

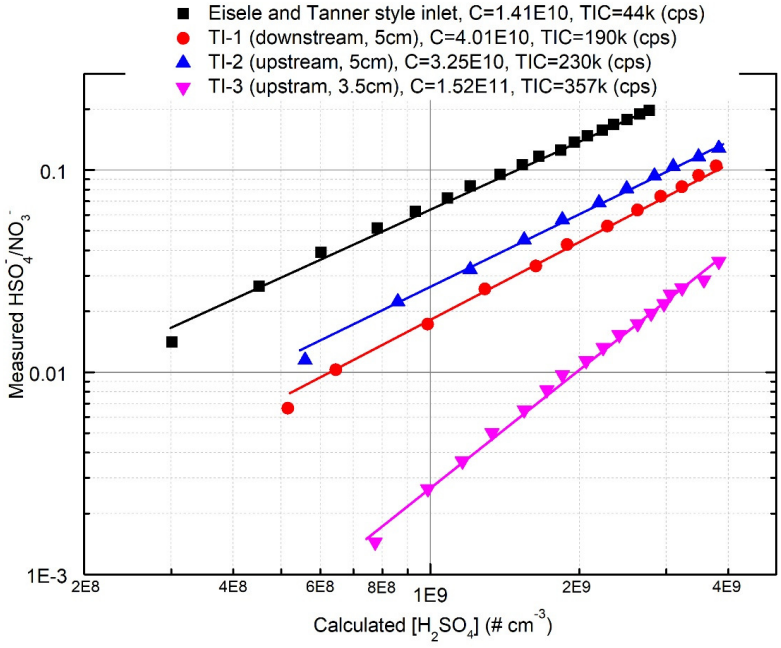

627

628 **Figure 3. Comparison of the sensitivities for the two inlets to H_2SO_4. The calibration process followed that reported by Kurten et al.**

629 **(2012) and is discussed in detail in the supplementary material. TI-1, 2, 3 represent different locations of the ion source relative to**

630 **the inlet orifice of the mass spectrometer. "upstream" and "downstream" indicated 0.5 cm upstream or downstream along the**

631 **sample flow axis and "3.5 cm" and "5 cm" indicate 3.5 or 5 cm away from the inlet orifice along the reagent ion flow axis.**

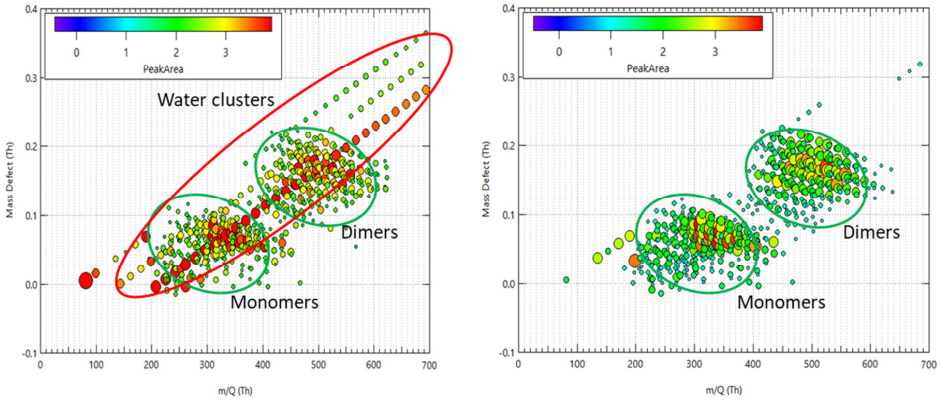

632

633 **Figure 4. Mass defect plots of α-pinene ozonolysis HOMs with 0 LPM (left) and 1 LPM (right) N_2 curtain gas flow when RH> 85%,**

634 **with monomer and dimer HOMs circled in green. The most intense ions comprising 60% of the total ion count are plotted for**

635 **clarity. H_2O clusters $(H_2O)_m(HNO_3)_nNO_3^-$ (m=1~30, n=0~2) are circled in red in the left plot and are notably absent with the**

636 **application of the N_2 curtain gas. $(HNO_3)_2NO_3^-$ and $HNO_3NO_3^-$ are much more likely to cluster with H_2O than NO_3^-.**

637

Atmos. Chem. Phys. Discuss., https://doi.org/10.5194/acp-2018-898
Manuscript under review for journal Atmos. Chem. Phys.
Discussion started: 10 September 2018

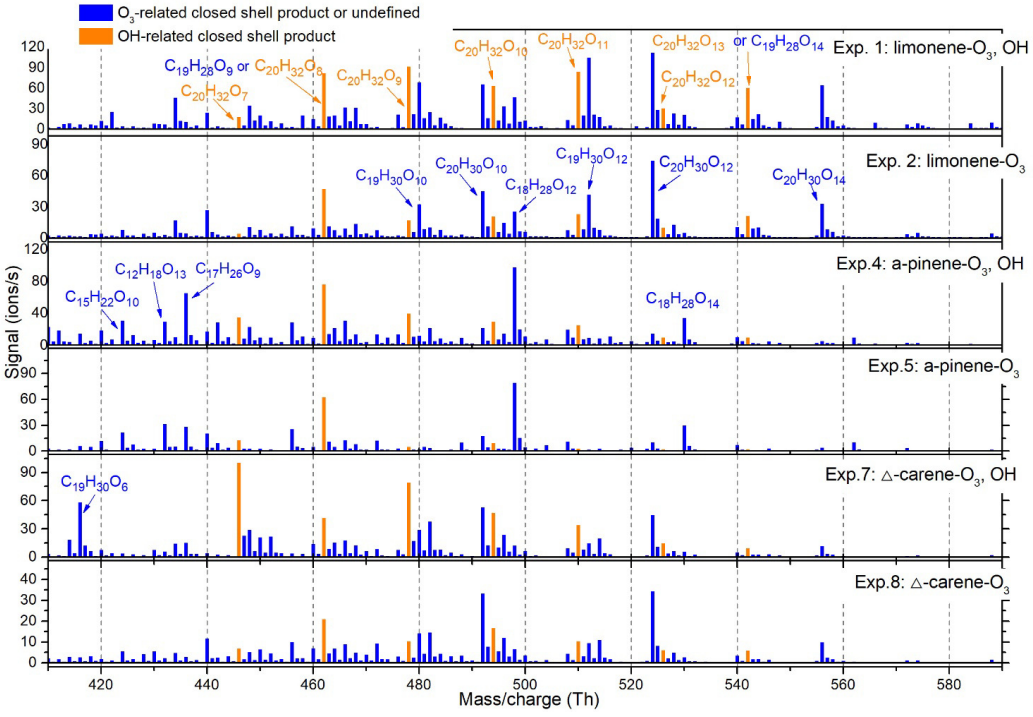

Figure 5. Average dimer mass spectrum in each of the particle generation experiments. The OH- and O_3-derived species were distinguished by comparing relative abundance of experiments with and without OH scavenger. All the peaks shown were in the form of adducts with NO_3^- or $HNO_3NO_3^-$ reagent ions.

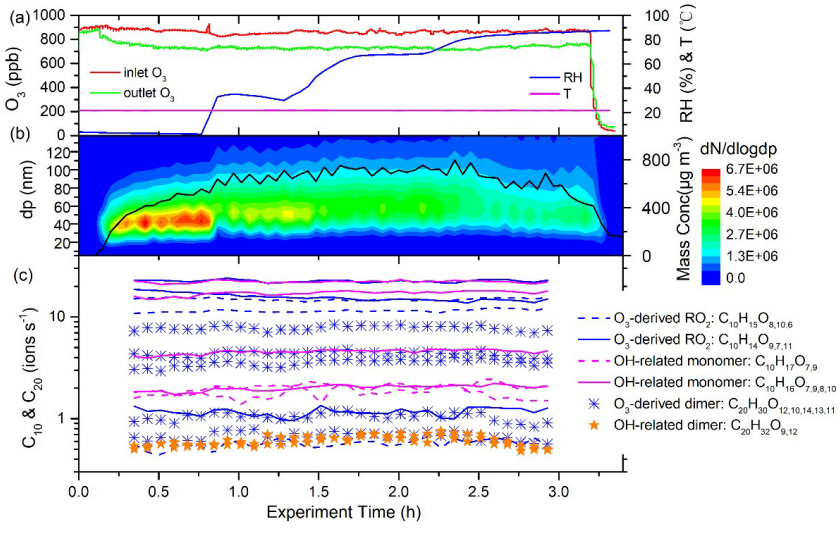

Figure 6. Time series of experimental parameters, particle size distribution, and key ions during EXP. 2 (limonene oxidized by O_3 without OH scavenger). (a) inlet and outlet O_3 concentrations, temperature, and RH; (b) Particle size distribution and integrated

Atmos. Chem. Phys. Discuss., https://doi.org/10.5194/acp-2018-898
Manuscript under review for journal Atmos. Chem. Phys.
Discussion started: 10 September 2018

Atmospheric Chemistry and Physics Discussions

646 **mass concentrations (assuming effective density is 1.2 g cm^{-3}); (c) Some of the main HOMs detected by TI-CIMS with NO_3^- reagent**
647 **ion. The subscript oxygen numbers in the formulae were ranked (left-to-right) according to signal abundance of the corresponding**
648 **molecule.**
649

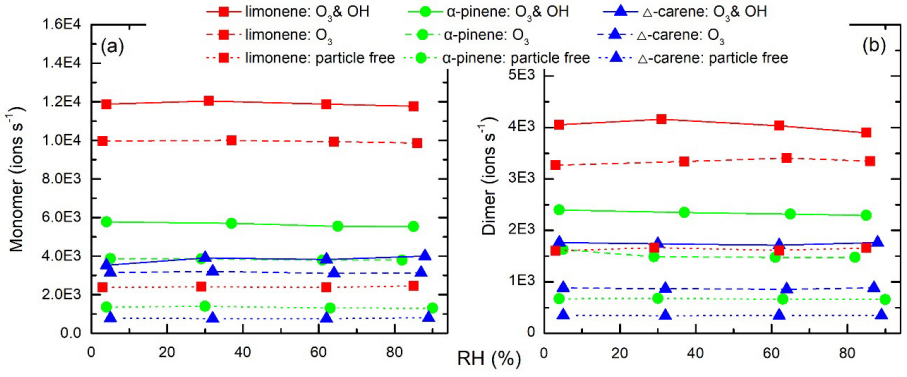

650
651 **Figure 7. Average (a) monomer and (b) dimer HOMs signal intensity (ions s^{-1}) as a function of RH in each experiment. Monomer**
652 **signals were the sum of C_{5-10} molecules and dimer signals were the sum of C_{15-20} molecules. No obvious signal change was seen for**
653 **increasing RH in any of the experiments.**
654

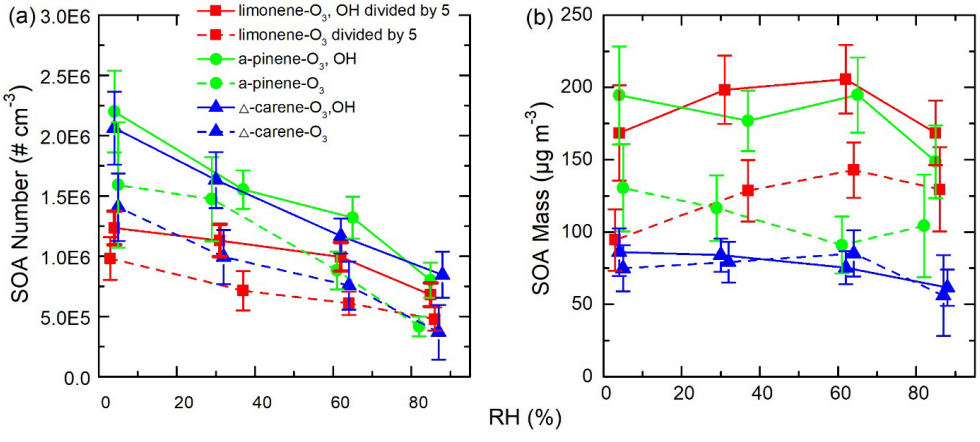

655
656 **Figure 8. SOA (a) number and (b) mass concentrations as a function of RH during different experiments. The error bars were**
657 **calculated using both the statistical errors of all individual size distributions during each RH stage and assuming a systematic CPC**
658 **counting error of 10%).**
659

Atmos. Chem. Phys. Discuss., https://doi.org/10.5194/acp-2018-898
Manuscript under review for journal Atmos. Chem. Phys.
Discussion started: 10 September 2018

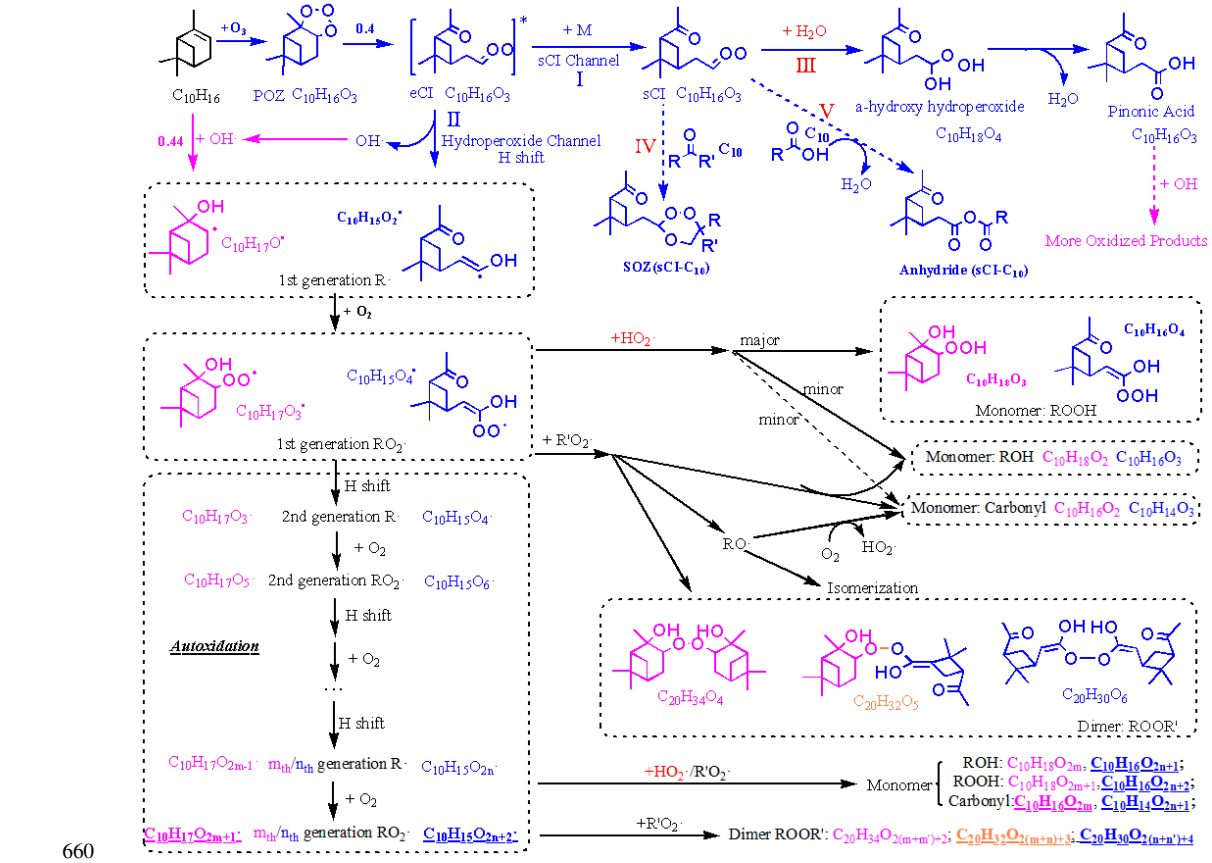

Figure 9. Proposed key steps in the formation of the representative C_{10} and C_{20} closed shell products from α-pinene oxidation and possible water vapor influence. Dashed lines represent pathways that may or may not happen, depending on the situation. Pink and blue colors represented the pathways or products from O_3 and OH oxidation, respectively. Common pathways or products are indicated in black type. Orange colors represented the combined products of O_3 and OH chemistry. Red colors highlight the direct or indirect influence of water. Underlined formulae were the main products observed from the mass spectrum. $C_{10}H_{18}O_{2m}$ and $C_{20}H_{34}O_{2(m+m')}$ were not observed in our spectrum, but they dominated the spectrum in other reported experiments where extra OH was generated (Berndt et al., 2016).

Atmos. Chem. Phys. Discuss., https://doi.org/10.5194/acp-2018-898
Manuscript under review for journal Atmos. Chem. Phys.
Discussion started: 10 September 2018

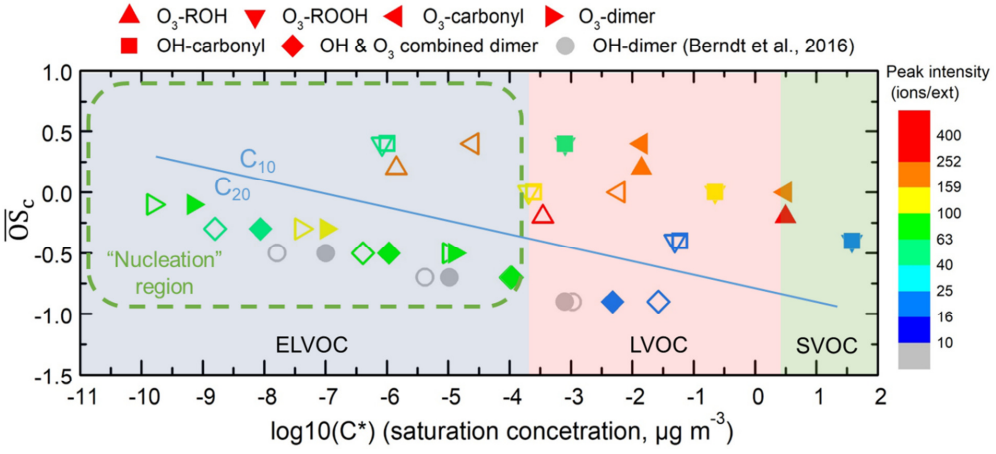

Figure 10. Vapor saturation mass concentration C* (T=298 K) of the major C_{10} and C_{20} closed shell products were predicted with SIMPOL.1 (open points) (Pankow and Asher, 2008) and Molecular Corridor method (filled points) (Li et al., 2016). O_3-derived, OH-related and OH-derived monomers and dimers are presented in different shapes. The peak intensity, represented by color, is from Exp.1 (limonene oxidation without OH scavenger). The gray points, which represent OH-derived dimers, are dominating products in OH initiated oxidation experiments (Berndt et al., 2016) while not observed in this study. Data used in this figure are given in Table S1. The nucleation region is from Donahue et al. (2013).